Journal of Power Sources 183 (2008) 619–628

Contents lists available at ScienceDirect

Journal of Power Sources

journal homepage: www.elsevier.com/locate/jpowsour

# Degradation analysis and modeling of reinforced catalyst coated membranes operated under OCV conditions

Sumit Kundu[a], Michael W. Fowler[a,*], Leonardo C. Simon[a], Rami Abouatallah[b], Natasha Beydokhti[b]

[a] Department of Chemical Engineering, University of Waterloo, 200 University Avenue West, Waterloo, Ontario, Canada N2L 3G1
[b] Hydrogenics Corporation, 5985 McLaughlin Road, Mississauga, Ontario, Canada L5R 1B8

ARTICLE INFO

*Article history:*
Received 10 March 2008
Received in revised form 28 May 2008
Accepted 29 May 2008
Available online 3 June 2008

*Keywords:*
OCV
Degradation model
PEMFC
Chemical degradation
Reinforced membrane

ABSTRACT

This paper studies the degradation of Gore™ PRIMEA® series 5510 catalyst coated membranes with an ePTFE reinforcement layer under open circuit voltage conditions at 90 °C, 75% RH, and no backpressure. Scanning electron microscopy (SEM) imaging of cross-sections revealed extensive cathode-side ionomer degradation and the presence of a platinum band. Cumulative fluoride release measurements show more fluoride exiting with the cathode effluent. Furthermore, both anode and cathode cumulative fluoride release plateau after long degradation times. Open circuit voltage was also monitored and the degradation rate was found to decrease after a long duration. It is proposed that all fluoride species are generated from the cathode-side ionomer degradation process and that the fluoride then diffuses to the anode and cathode channels. Further, once the cathode-side ionomer is consumed the degradation reaction slows as the "degradation front" passes through the inert reinforcement layer. This process was modeled using a semi-empirical transient model and compared to experimental results.



## 1. Introduction

Fuel cell durability is one of the current limitations preventing wide scale commercialization of polymer electrolyte membrane (PEM) technology. Though there are many parts of a fuel cell system that can influence reliability and durability, the degradation of the membrane electrode assembly (MEA), and in particular the polymer electrolyte, is the most important. Not only is the membrane one of the most vulnerable components in a typical fuel cell, but it is also one of the most expensive and therefore important to preserve in an application. For these reasons it is essential to understand how and where the membrane degrades in a fuel cell.

The fuel cell degradation process can be broadly summarized into causes, modes, and effects [1]. There are many causes resulting in the failure of polymer electrolyte membranes ranging from manufacturing and design issues such as over-compression or membrane thickness variability [2], material properties such as swelling [3,4], and particularly from the operational conditions that the fuel cell is required to run under such as high and low humidity and even sub-zero temperatures [5–7]. Each cause results in failure through a particular degradation mode. These modes can be classified as chemical, mechanical, and thermal modes [1,2,8].

### 1.1. Chemical degradation of electrolyte membranes

Chemical degradation of the ionomer membrane, caused by gas crossover, is a significant degradation pathway of the MEA. This type of degradation generally leads to failure by compromising the integrity of the ionomer membrane. Interestingly, in addition to being the cause of degradation issues, gas crossover is also used as an indicator for membrane integrity whereby a threshold value for the amount of gas crossover based on safety of operation dictates if a fuel cell has reached the 'failure' point.

In the case of Nafion™ it has been proposed that carboxylic acid end groups left over from the manufacturing process may be susceptible to attack by radical species [9] generated during fuel cell reactions. The proposed mechanism is as follows:

Step 1: $R\text{-}CF_2COOH + OH^{\bullet} \rightarrow R\text{-}CF_2^{\bullet} + CO_2 + H_2O$
Step 2: $R\text{-}CF_2^{\bullet} + OH^{\bullet} \rightarrow R\text{-}CF_2OH \rightarrow R\text{-}COF + HF$
Step 3: $R\text{-}COF + H_2O \rightarrow R\text{-}COOH + HF$

The radical species, such as hydroxyl radicals, are thought to be formed by the decay of hydrogen peroxide or by the oxygen reduction reaction. It has been proposed that hydrogen or oxygen crossover may lead to peroxide and radical generation facilitating

* Corresponding author. Tel.: +1 888 4567x33415; fax: +1 519 746 4979.
*E-mail addresses:* s2kundu@uwaterloo.ca (S. Kundu), mfowler@uwaterloo.ca (M.W. Fowler).

0378-7753/$ – see front matter © 2008 Published by Elsevier B.V.
doi:10.1016/j.jpowsour.2008.05.074

**Nomenclature**

| | |
|---|---|
| $C_{F^-}$ | fluoride ion concentration (mol cm$^{-3}$) |
| $D_{GDL}$ | fluoride diffusion coefficient through the GDL (cm$^2$ s$^{-1}$) |
| $D_i$ | diffusion coefficient of species $i$ (cm$^2$ s$^{-1}$) |
| $D_I$ | fluoride diffusion coefficient through the ionomer (cm$^2$ s$^{-1}$) |
| $E_{Nernst}$ | Nernst potential (V) |
| $E_{OCV}$ | open circuit voltage (V) |
| EAS | electrochemically active surface area per unit geometric surface area (m$^2$ m$^{-2}$) |
| EAS$^o$ | initial electrochemically active surface area per unit geometric surface area (m$^2$ m$^{-2}$) |
| $f_I$ | cathode ionomer fraction |
| $F$ | Faraday's constant (C mol$^{-1}$) |
| $F_C$ | cumulative fluoride release per unit geometric surface area (mol cm$^{-2}$) |
| $i_{H_2}$ | crossover current per unit geometric surface area (A cm$^{-2}$) |
| $i^o_{H_2}$ | initial crossover current per unit geometric surface area (A cm$^{-2}$) |
| $i_o$ | exchange current density per active surface area (A cm$^{-2}$) |
| $k_{H_2}$ | hydrogen permeability constant (mol cm cm$^{-2}$ mmHg$^{-1}$ s$^{-1}$) |
| $k'_{H_2}$ | hydrogen permeability constant (A cm cm$^{-2}$ mmHg$^{-1}$) |
| $K_1$ | proportionality constant (cm$^2$ mol$^{-1}$) |
| $K_2$ | proportionality constant (mol cm$^{-2}$) |
| $K_3$ | proportionality constant |
| $n_{F^-}$ | moles of fluoride ion per geometric surface area (mol cm$^{-2}$) |
| $N_{F^-}$ | fluoride ion flux (mol cm$^{-2}$ s$^{-1}$) |
| $N_{H_2}$ | hydrogen flux (mol cm$^{-2}$ s$^{-1}$) |
| $N_{OH}$ | OH radical flux (mol cm$^{-2}$ s$^{-1}$) |
| $R$ | ideal gas constant (J mol$^{-1}$ K$^{-1}$) |
| $T$ | temperature (K) |
| $x$ | distance from anode channel (cm) |

*Greek symbols*

| | |
|---|---|
| $\gamma$ | crossover current modifier |
| $\delta$ | total ionomer membrane thickness (cm) |
| $\delta_{IA}$ | anode ionomer thickness (cm) |
| $\delta^o_{IC}$ | initial cathode ionomer thickness (cm) |
| $\Delta p_{H_2}$ | hydrogen pressure differential (mmHg) |
| $\eta_{Crossover}$ | voltage loss due to hydrogen crossover (V) |
| $\eta_{irreversible}$ | irreversible voltage loss (V) |
| $\eta_{reversible}$ | reversible voltage loss (V) |

the degradation of the ionomer membrane [2,9–12]. One of the products of the degradation reaction shown is HF which would exit the fuel cell in the effluent water.

The link between crossover and membrane degradation has been investigated by several groups. Aoki et al. [13,14] experimented with hydrogen/air mixtures simulating hydrogen rich or oxygen rich environments to study the degradation of ionomer membranes in the presence of platinum. They found that in both cases degradation of the ionomer membrane, as revealed by the production of fluoride ions, occurred and therefore it was possible for crossover hydrogen and oxygen to degrade the fuel cell membrane. Degradation was only observed in the presence of platinum in this study. They also observed that an increase in relative humidity (RH), while keeping dry gas partial pressures constant, increased the fluoride release rate. This was attributed to the increase in gas permeability of the membranes. Mittal et al. [15] also studied how hydrogen and oxygen crossover may degrade the membrane. They suggested that the degradation mechanism does not depend on the potential of the electrodes but instead is simply chemical in nature. They also found that an increase in the relative humidity of the gasses decreased the degradation rate. This was attributed to RH impacting the catalyst surface, and somehow impeding the peroxide formation reaction.

One method of studying chemical degradation is through the use of an open circuit voltage durability experiment. The premise of this experiment is to hold a fuel cell at open circuit conditions (i.e. where no load is being drawn) while flowing hydrogen and oxygen (or air) as reactants. Since there is no consumption of reactants gas partial pressures remain high throughout the fuel cell, which creates the driving force for gas permeation across the membrane. This has been shown to be true using models by several authors [16–18]. The increased permeation rates are thought to degrade the membrane chemically as discussed previously. There have been an increasing number of publications related to OCV tests in the literature. There is some debate as to where the majority of peroxide involved in degradation is produced in the membrane and where degradation within the membrane is most severe. Common measurements in these experiments are fluoride release, gas crossover, as well as open circuit voltage degradation rates. All three of these measures are inter-related. As a membrane degrades it will release fluoride ions at the same time hydrogen crossover will increase with degradation. It is widely accepted that the deviation of operational OCV and theoretical OCV is due to a mixed potential effect caused by hydrogen crossover. It has typically been modeled as a modified Tafel equation [18–20]. As hydrogen crossover increases through a membrane the open circuit voltage will become lower.

Hommura et al. [21] used a Flemion$^{TM}$ membrane and severe durability conditions (120 °C and 17% RH) in an OCV test. They found that the open circuit voltage decreased considerably over 160 h from 0.95 V to less than 0.65 V while the hydrogen crossover rate increased almost exponentially. Endoh et al. [6] performed an OCV durability experiment at low cathode RH with 100% anode RH. They used electron spin resonance (ESR) to identify carbon radicals which they theorized to have come from degradation of the carbon catalyst support by radical species. Other OCV tests by Inaba et al. [22] found that the cell fluoride emission rate was more significantly impacted by changes in the oxygen partial pressure and less for the hydrogen partial pressure. From this they indicated that oxygen crossover to the anode may be more important to membrane degradation than hydrogen crossover. Unfortunately the work was not complimented with a forensic analysis of the membrane to determine the extent to which it had thinned or if pin holes caused increased crossover. Other studies by Mittal et al. [23] and Chen and Fuller [24] show that peroxide and chemical degradation can be produced at either electrode by operating cells in "anode only" and "cathode only" modes.

It has recently been reported by Liu et al. [25], Ohma et al. [26,27], and Bi et al. [28] that platinum from the cathode catalyst may dissolve under OCV conditions and migrate into the polymer electrolyte membrane and then redeposit. The location of the deposits depends largely on the partial pressures of hydrogen and oxygen as well as their permeability, though for most common systems involving pure hydrogen and air, the deposits are close to the cathode side. Liu and Ohma further proposed that the platinum within the ionomer allows for the production of radical species that then degrade the membrane. It is still difficult to postulate

if the deposits are the result of the degradation process or if they are facilitating the process. There has been recent work by Endoh et al. who did not find a correlation between membrane degradation as seen by FTIR analysis of cross-sections and the location of the platinum band [29].

There have been few OCV degradation experiments to study chemical degradation on reinforced membranes in the literature. Use of a reinforced membrane offers two advantages. First, the reinforcement layer allows identification of the region of degradation as being close to the cathode or close to the anode. Also, the reinforcement layer offers improved mechanical stability so that the membrane does not fail due to a mechanical rip, tear, or breach and instead can be degraded chemically for long periods of time. Paik et al. [3] performed OCV durability tests on Gore™ membrane electrode assemblies and operated at 90 °C and 100% and 30% RH for the anode and cathode gas streams, respectively. They found that the reduced relative humidity also reduced the lifetime of the fuel cell and their presented data indicated that at 100% RH the rate of OCV degradation slows considerably with time. Pure oxygen was used as the cathode gas. The improved durability at higher relative humidity was attributed to lower gas partial pressures, preventing degradation from crossover. The work by Paik did not examine the membrane after degradation.

### 1.2. Membrane degradation modeling

Though there have been some stochastic degradation models [30] developed to predict how key fuel cell properties change with age (independent of degradation mode), there have been few attempts to model the chemical degradation processes in a fuel cell. Teranishi et al. [31] made one such attempt. They performed an OCV test which lasted 24 h and observed voltage decay. Their scanning electron microscope studies indicated that over the testing time the cathode catalyst layer/membrane interface had become weakened. They performed experiments at 100 and 0% RH and they concluded that the degradation of OCV was caused by a reduction in electrochemically active surface area with the aid of an OCV model. However they did not attempt to model the degradation process itself.

This paper examines the degradation of a reinforced membrane and attempts to model the effects. A Gore™ PRIMEA® series 5510 catalyst coated membrane with an ePTFE reinforcement layer was degraded under open circuit voltage conditions to enhance chemical degradation. The study uses scanning electron imaging of cross-sections, cumulative fluoride release measurements, and open circuit voltage degradation to propose a degradation process. This process is then modeled using a semi-empirical transient model and compared to experimental results.

## 2. Experimental

### 2.1. Fuel cell materials and testing apparatus

The single cell fuel cell tested was made by Hydrogenics Corporation and had a geometric active area of 80.1 $cm^2$. The cell was assembled using Gore™ PRIMEA® series 5510 catalyst coated membranes (CCM) and proprietary gas diffusion layers (GDL) with a microporous layer (MPL). The ionomer membrane contained an ePTFE reinforcement which increases mechanical stability of the membrane. The cell was tested on a Hydrogenics FCATS™ test station which controlled temperature, humidity, and gas flows. The cell underwent a break-in period of 8 h prior to OCV durability testing. During break-in, cell voltage was kept at approximately 0.6 V.

### 2.2. Open circuit voltage test

Open circuit voltage (OCV) durability test was conducted at 90 °C, 75% anode/cathode relative humidity, and no backpressure. Pure hydrogen was used on the anode and air on the cathode. Anode flow rate was 0.2 SLPM and cathode flow rate was 0.8 SLPM. Knock-out drums were used on the fuel cell outlets to condense and collect water during fuel cell operation. Water samples were collected daily and were kept in polyethylene bottles prior to analysis.

### 2.3. Fluoride ion chromatography

Fluoride ion analysis was carried out with a Dionex ED40 electrochemical detector working with a Dionex GP40 gradient pump. The minimum detectable fluoride ion concentration was 0.011 ppm $F^-$.

### 2.4. Scanning electron microscopy

SEM analysis was carried out using a LEO SEM with field emission Gemini Column. The gas diffusion layers were first removed from the membrane electrode assemblies. This was done by repeatedly heating, humidifying and then cooling the MEA until the GDL could be removed easily. Cross-sections were made by freeze fracture from a strip of sample submerged in liquid nitrogen. Once frozen, the sample was broken in half while still submerged. Samples were also sputter coated with gold to improve conductivity. SEM images were later analyzed with Scion Image Analysis software to obtain estimates of layer thicknesses.

### 2.5. Electrochemical characterization

Crossover current measurements were performed using an EG&G Princeton Applied Research potentiostat/galvanostat model 273 and Coreware software. Humidified hydrogen was passed on the anode, and humidified nitrogen was supplied to the cathode. Crossover current measurements were conducted with a sweep rate of 2 mV $s^{-1}$. Electrochemical characterization tests were conducted very sparsely over the course of the experiments. This was done to minimize voltage recovery phenomena experienced when the cell conditions were changed or the cell was shut down [32].

### 2.6. Gas crossover

Crossover measurement of oxygen and hydrogen were manually measured by pressurizing the anode side of the fuel cell to 5 psi of the test gas and measuring the crossover rate. From this information an estimate of the permeability was obtained. Measurement were conducted at room temperature with fully humidified gasses. The permeability, $k_i$, was determined from the differential pressure, $\Delta p_i$, membrane thickness, $\delta$, and the molar flux across the membrane, $N_i$, as shown in Eq. (1) below.

$$N_i = k_i \frac{\Delta p_i}{\delta} \quad (1)$$

## 3. Results and discussion

### 3.1. Initial Gore™ membranes—terminology and crossover

The reinforced catalyst coated membrane used in this study consists of several layers which require defining. Fig. 1 is a scanning electron microscope (SEM) image identifying the 5 main layers of a Gore™ PRIMEA® series 5510 CCM. The most distinguishing feature of these membranes is the ePTFE reinforcement layer at the

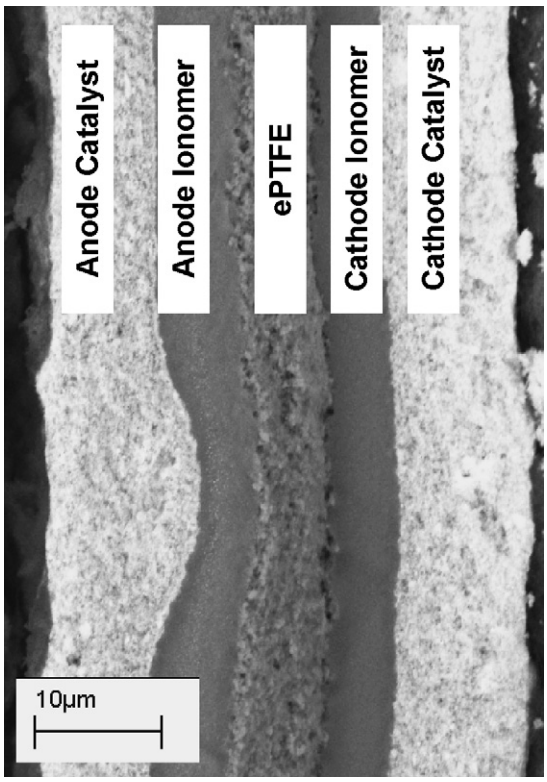


**Fig. 1.** SEM cross-section of a fresh Gore$^{TM}$ reinforced catalyst coated membrane.

centre of the membrane. The reinforcement layer is a porous ePTFE membrane and is discussed in the literature [33]. Since this layer bisects the ionomer membrane, the ionomer closest to the anode will be referred to as the anode ionomer, and ionomer closest to the cathode will be referred to as the cathode ionomer. It should be noted that anode and cathode ionomer do not refer to ionomer that may be present within the catalyst layer as a binder. Initially, anode and cathode ionomer layers have similar thicknesses measuring between 4 and 6 μm. The reinforcement layer thickness ranged between 6 and 7 μm. The total thickness of CCM is approximately 50 μm.

Hydrogen permeation across the CCM was measured by crossover current. Since hydrogen permeability is a function of the hydration and temperature of the membrane [2,34,35], measurements were taken at the temperature and humidification conditions of the experiment (in this case 90 °C, 75% RH). A typical crossover current curve is shown in Fig. 2, the current stabilized at 0.143 A or 1.8 mA cm$^{-2}$. Hydrogen and oxygen permeability was also measured in a separate test using conventional flow measurements. Those results showed that hydrogen was 2.6 times more permeable than oxygen.

### 3.2. Diagnostic tests

#### 3.2.1. Open circuit voltage performance

The cell open circuit voltage was monitored with testing time and is shown in Fig. 3. The voltage degradation curve displays several characteristics typical of Gore$^{TM}$ membrane degradation under OCV conditions [3,32]. First, there is an initial rapid drop in voltage followed by stabilization. Interruption of the testing, for polarization curve measurement, causes voltage recovery.

The first 460 h ran continuously without interruption. From 460 to 860 h the experiment was stopped several times. The initial voltage drop during the first 100 h is mostly attributed to recoverable processes as described in previous work [32]. Overall the voltage dropped from 0.9 V to approximately 0.77 V. There was little observed voltage degradation between 380 and 460 h. Further, between 460 and 860 h, despite the high degree of scatter caused by the more frequent stoppages, the voltage was observed to remain around 0.77 V, also indicating little voltage degradation.

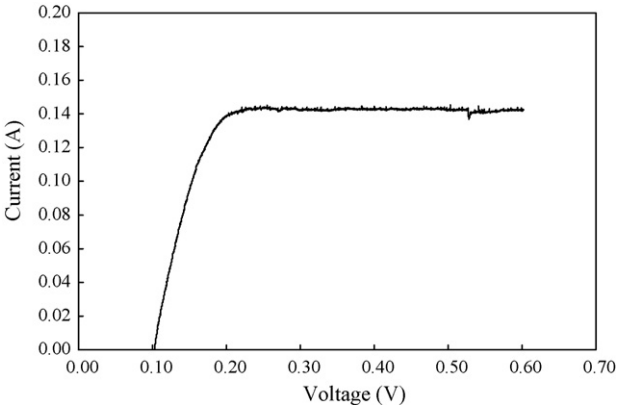


**Fig. 2.** Crossover current curve for Gore$^{TM}$ CCM at 90 °C, 75% RH, and no backpressure using 2 mV s$^{-1}$ scan rate.

#### 3.2.2. Fluoride release

Effluent water was collected from both anode and cathode sides of the fuel cell and fluoride ion concentration was measured using ion chromatography. Using measurements of the total amounts of water collected, the cumulative fluoride release as well as the fluoride release rates could be determined and are shown in Fig. 4a and b, respectively. There are several sections of the cumulative fluoride release curve, Fig. 4a, of note. Both anode and cathode curves begin with a slow exponential rise, this is followed by a linear increase, and finally the anode and cathode fluoride release appears to reach an upper limit. This is also reflected in the release rate data (Fig. 4b) which shows that fluoride release rates peak at approximately 150 h which is consistent with data published by Liu et al. [36] who used similar Gore$^{TM}$ membranes as in this study. Finally, cathode cumulative release is higher than anode cumulative release.

Water balance calculations were conducted to determine if there was any net water flow from the anode to the cathode which could be involved in transporting ions across the membrane. Over the course of the experiment, measured cathode and anode effluent water flow rates ranged between 15–40 and 9–13 mL h$^{-1}$, respec-

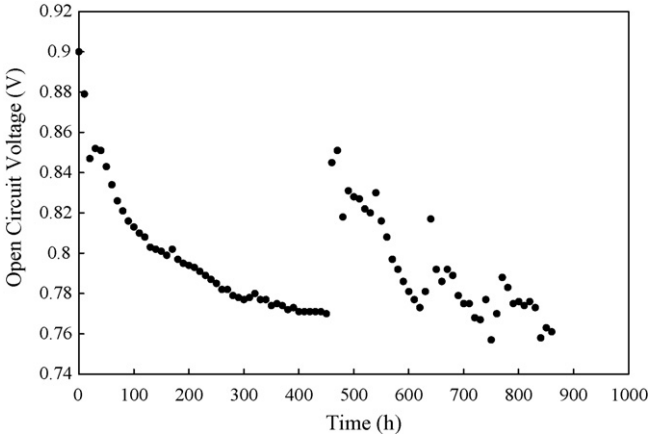


**Fig. 3.** OCV durability data at 90 °C, 75% RH, and no backpressure.

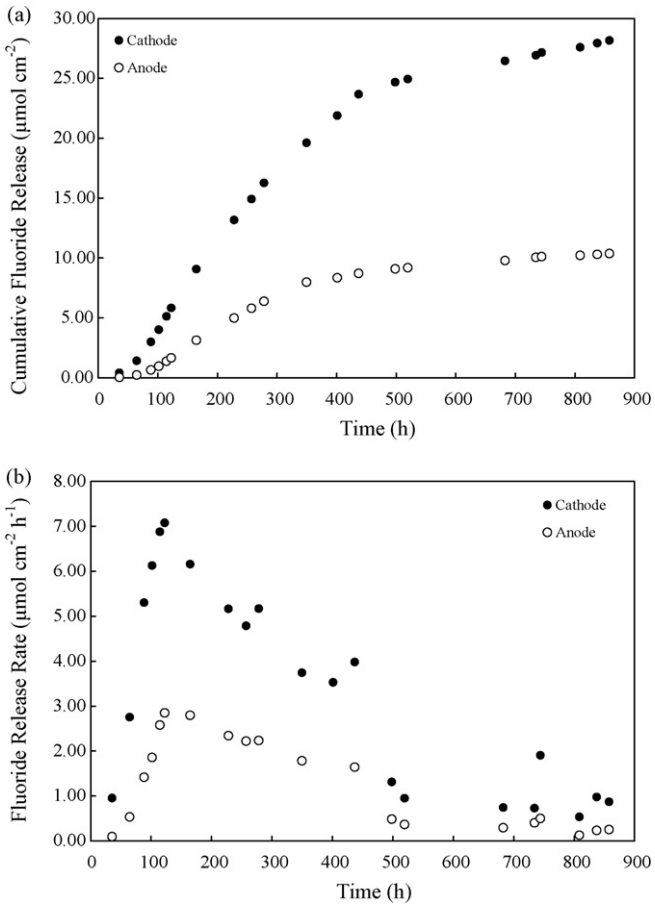


**Fig. 4.** Anode and cathode (a) cumulative fluoride release and (b) fluoride release rates during the duration of testing.

tively. Calculated rates based on inlet RH and gas flow rate were determined to be 32.9 and 12.1 mL $h^{-1}$ for the cathode and the anode sides, respectively. The bulk of the measurements were similar to the theoretical values as shown in Fig. 5 and deviations are attributed to ambient temperature fluctuations or water collection errors. From this data there is no evidence of net water transport from the anode or cathode indicating that it was not a factor in fluoride ion transport.

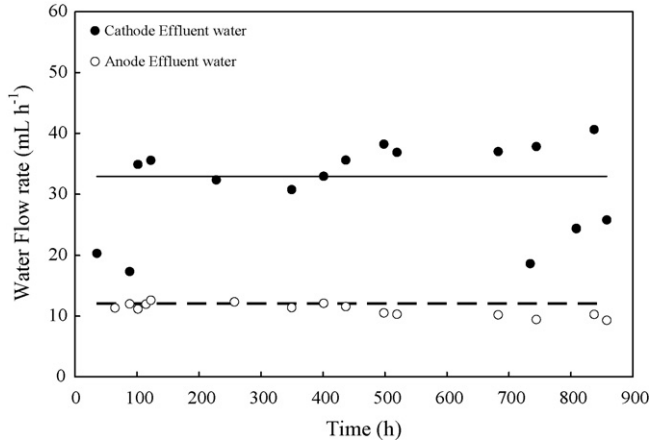


**Fig. 5.** Effluent water flow rates. Solid and dotted lines represent theoretical values.

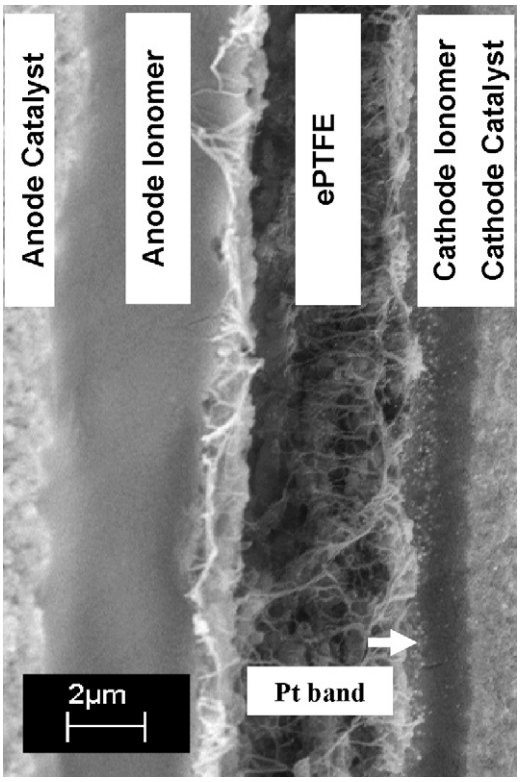


**Fig. 6.** Typical cross-section of the aged CCM after 860 h, 5000× magnification.

### 3.2.3. Crossover current measurements

Due to the voltage recovery, which happens when cell operation is interrupted in these particular cells [32], crossover measurements were only done at the beginning of life (BOL), and after 460 h. Between these times the crossover increased from 1.8 to 3.5 mA $cm^{-2}$.

## 3.3. Scanning electron microscopy results

Forensic analysis of the CCM, consisting mainly of SEM imaging, allowed visualization of the effects of degradation. These forensic results will be used to understand the trends in diagnostic testing results which were described in the previous section.

After testing, the MEA was removed from the fuel cell hardware. The membrane was observed to have maintained mechanical integrity with no visible rips or tears. SEM images of cross-sections from nine evenly distributed locations over the membrane area of the cell were taken. Fig. 6 shows a typical cross-sectional image of the CCM after 860 h of operation. The cathode and anode catalyst layers are clearly visible as is the reinforcement layer. The anode ionomer layer is also visible and well defined however the cathode ionomer layer shows significant thinning which is considered to be a sign of chemical degradation. Measurements with Scion Image Analysis software revealed that the anode ionomer had an estimated average thickness of 3.6 μm and the cathode ionomer had an average thickness of <1 μm after 860 h. This result indicates that the cathode ionomer degrades much more rapidly and extensively than the anode ionomer. It was also observed that areas where the anode ionomer had thinned appreciably were only in areas where the cathode ionomer had degraded extensively. This suggests that the anode ionomer degrades only after the cathode ionomer has degraded significantly.

One explanation for the severity of the cathode ionomer degradation is that the membrane is more permeable to hydrogen than

oxygen. This, in addition to the partial pressure of hydrogen also being higher than oxygen under the stated conditions, means that hydrogen crossover will dominate and therefore degradation reactions at the cathode will also dominate. Under the test conditions, 75% RH and a total pressure of 760 mmHg, the partial pressure of hydrogen is 364 mmHg while the partial pressure of oxygen in air at 75% RH and 760 mmHg is only 77 mmHg. From initial permeability experiments it was also found that hydrogen permeability is 2.6 times greater than oxygen permeability. Application of Eq. (1) shows that the overall crossover rate of hydrogen can be expected to be 12 times greater than the crossover of oxygen.

Analysis of the SEM images also reveals platinum deposits in the cathode ionomer. It is not yet clear if the platinum deposits are a result of the degradation process or if they facilitate degradation. Recent work [25–27] has suggested that the platinum deposits are responsible for catalyzing the production of radical species in the membrane. Furthermore, it was postulated that higher hydrogen crossover causes the platinum band to appear close to the cathode. This is consistent with the observed cathode ionomer degradation since the Pt band was only observed in the cathode ionomer.

### 3.4. Degradation process

There are several observations from the SEM analysis and fluoride release data which, to the author's knowledge, have not been adequately explained or observed in the literature. First, degradation as observed by membrane thinning has occurred severely on the cathode ionomer. Second, fluoride ions were detected in both the anode and cathode effluent water. Mechanical creep can cause thinning, however, it would not explain why only cathode thinning is seen and the fluoride release trends. It may also be suggested that degradation processes are occurring on the anode and cathode sides simultaneously, a third observation that both fluoride release curves begin to plateau at the same time indicates that all the fluoride is generated at a common reaction location. This is also mirrored in the observation that OCV stabilized after a period of degradation.

To rationalize the SEM and cumulative fluoride release data it is proposed that degradation, and hence the generation of fluoride ions, occurs on the cathode side, where radical species are produced at the catalyst layer/ionomer membrane interface. This is consistent with recent studies by Liu et al. [25], Ohma et al. [26,27], and Bi et al. [28]. It is further proposed that a "degradation front" will move through the cathode ionomer until it reaches the reinforcement layer. Once all the cathode ionomer is consumed the reactions that generate fluoride will stop until the front is able to move through the reinforcement layer and begin degrading the anode. The reinforcement layer itself does not degrade however the ionomer within it will degrade if radicals are able to penetrate to ionomer locations from the generation point. The fluoride produced on the cathode side may be transported out of the cell by two paths as depicted in Fig. 7. The first path (Path 1) considers fluoride diffusing from the generation point, through the cathode GDL/MPL and to the cathode channels. The second path (Path 2) requires that the fluoride ions diffuse through the ionomer membrane as well as the anode GDL/MPL to reach the anode channels. There is still some ambiguity as to where the peroxide is generated and therefore the crossover of which as species will control degradation. Studies have shown that peroxide may be generated at the anode from crossed-over oxygen and then diffuse to the cathode, or be generated at the cathode by crossover hydrogen [23,24]. For the following modeling attempt it will be assumed that the peroxide responsible for radical generation and degradation is produced near the degradation location, in this case at the cathode catalyst layer.

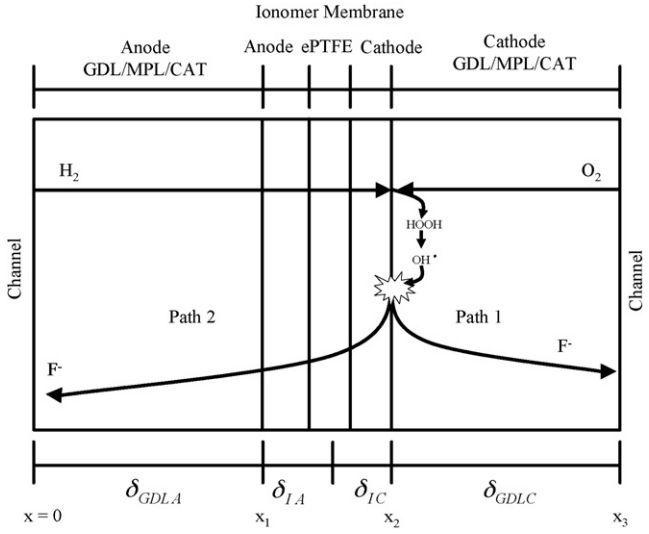


**Fig. 7.** Model domain and processes.

This mechanism is supported by the SEM data which suggests that the cathode ionomer degrades before the anode ionomer. It also explains why the cumulative cathode fluoride release is much higher than the cumulative anode fluoride release since there would be less diffusion resistance, because of the shorter path length, following Path 1 rather than Path 2 and consequently fluoride would preferentially diffuse via Path 1. Finally this mechanism also explains why anode and cathode fluoride release curves plateau at the same time. Since all fluoride is being produced by a reaction between radicals and the cathode-side ionomer, when the ionomer has been depleted the fluoride production rate would be expected to slow or stop. It is possible that once the cathode ionomer is severely degraded anode degradation may become significant since radicals generated at the cathode may be able to diffuse through the reinforcement layer to the anode ionomer. The reason why the cathode degradation is dominant is attributed to the higher driving force for hydrogen permeation over oxygen permeation as previously discussed.

A final feature of the cumulative fluoride release curves is the initial lag time. This is attributed to the time delay between the production of fluoride ions within the ionomer and movement into the channel caused by the resistance to diffusion in both paths. The path to the anode channel (Path 2) has higher resistance because of the extra layers of material to diffuse through and hence would have a longer lag time. This explanation is consistent with the cumulative fluoride release observations.

The OCV data can also be similarly interpreted. Open circuit voltage has been shown to be related to hydrogen crossover [30]. As degradation of the ionomer proceeds it becomes thinner, hydrogen permeation increases, and hence OCV decreases. Once the cathode ionomer has been substantially degraded, the degradation slows. Since the degradation slows, the membrane ceases to thin, or the rate of thinning decreases substantially, and crossover rates can be expected to stabilize. As such, the open circuit potential will also stabilize.

## 4. Proposed degradation model formulation

To understand the mechanisms involved in the degradation process a semi-mechanistic 1D transient model is proposed. The overall purpose of this model is to provide a simple evaluation tool of the effects of membrane permeability and relative humidity

on cathode ionomer degradation, fluoride release, and open circuit voltage degradation, as well as identify parameters which help explain the experimental results. Further uses of this model include incorporation into system reliability models since it predicts membrane degradation with time.

This model incorporates degradation processes instigated by hydrogen crossover as well as the transport of fluoride ions in an attempt to model the experimental data. As discussed above, this initial modeling attempt assumes that peroxide generation occurs at the cathode and in controlled by hydrogen crossover. This will allow the general form of the model to be developed. This can be modified as data on the peroxide generation and transport mechanism become more fully understood. The system studied experimentally is highly complex, consisting of many different layers. In order to simplify the system four main areas will be considered as shown in Fig. 7. The anode and cathode GDL/MPL/catalyst layers will be two such blocks, the anode ionomer and ePTFE layer will be a third block, and cathode ionomer layer will be the final block. Degradation is considered to be at the cathode ionomer/catalyst interface where oxygen transport to the reaction sites is fast. It is also assumed that the ionomer and ePTFE layers within the membrane controls permeation of hydrogen from the anode to the cathode. At OCV conditions the reactant pressures are assumed to be uniform from the channels to the ionomer membranes.

The main processes modeled here are the permeation of hydrogen to the cathode catalyst/ionomer interface followed by the degradation of the cathode ionomer. This degradation process is modeled as a reduction in membrane thickness accompanied by the release of fluoride ions. Anode ionomer degradation is not considered at this time. The transport of fluoride ions is considered to diffuse through the various layers to either the cathode or anode channels (Path 1 and Path 2 as indicated in Fig. 7) where it is swept away. The impact of increased crossover with time, due to the reduction of thickness, and changes in electrochemically active surface area on open circuit potential are also modeled.

### 4.1. Membrane degradation and fluoride ion production

The rate of hydrogen crossover is determined by the permeability of the membrane, the partial pressure difference across the membrane and the thickness of the ionomer membrane layers. This hydrogen flux, $N_{H_2}$, can be calculated by (2) and is related to the crossover current measured during linear sweep voltammetry tests by (3).

$$N_{H_2} = k_{H_2} \frac{\Delta p_{H_2}}{\delta} \tag{2}$$

$$i_{H_2} = k_{H_2}(2F)\frac{\Delta p_{H_2}}{\delta} = k'_{H_2}\frac{\Delta p_{H_2}}{\delta} \tag{3}$$

Once at the reaction site, the hydrogen will react with oxygen to form peroxide species which will then form radicals. It has been assumed that hydrogen controls the rate of peroxide formation, and hence radical generation. As such, the rate at which radicals are produced will be proportional to the flux of hydrogen permeating through the membrane and can be described by (4).

$$N_{OH} \propto N_{H_2} \tag{4}$$

Once created, OH radicals will degrade the polymer electrolyte membrane producing fluoride ions as a byproduct. Consumption of the ionomer therefore depends of the rate of OH radical production as well as the amount of ionomer available for reaction. In this case the accessible polymer is the cathode ionomer since the ePTFE layer likely presents a barrier to OH radical diffusion to the anode ionomer layer. The rate of ionomer consumption will therefore be related to the rate of radical production and the fraction of remaining cathode ionomer, $f_I$, as shown in Eq. (5).

$$-\frac{df_I}{dt} \propto (N_{OH})(f_I) \tag{5}$$

Substituting the hydrogen flux and a proportionality constant yields Eq. (6):

$$-\frac{df_I}{dt} = K_1(N_{H_2})(f_I) \tag{6}$$

where $K_1$ is a proportionality constant, similar to a reaction rate constant, relating the hydrogen flux and ionomer fraction to the ionomer degradation rate. This degradation rate determines the rate of fluoride production as well as the rate of thickness change. The release of fluoride ions is related to the rate of ionomer degradation through the polymer chain structure. Since the exact chemical formula and molecular weight for the PFSA ionomer used in the tested membranes is proprietary and fluoride containing chain fragments may leave the fuel cell as degradation products the amount of fluoride ions generated for every percent of ionomer that has been degraded are related by a proportionality constant in Eq. (7). Physically this constant would be related to the number of fluorine in the ionomer chain structure.

$$\frac{dn_{F^-}}{dt} = -K_2\frac{df_I}{dt} \tag{7}$$

### 4.2. Fluoride ion transport

Fluoride ions, once generated, may be transported to the channels of the bipolar plates by two paths, Path 1 and Path 2, as previously discussed and shown in Fig. 7. Path 1 considers fluoride ion diffusion from the cathode ionomer/catalyst interface through the cathode GDL layer and ultimately to the cathode channels. Path 2 involves diffusion of fluoride ions from the cathode ionomer/catalyst interface, through the ionomer layer, the ionomer-filled ePTFE layer and the anode GDL layer to the anode channels. The rate at which these processes occur depends on the concentration gradients in the different layers. These gradients are time-dependant and are modeled as using Fick's law as shown in Eq. (8).

$$\frac{dC}{dt} = D_i\frac{d^2C}{dx^2}, \quad D_i = \begin{cases} D_{GDL}, 0 < x < x_1 \\ D_I, x_1 < x < x_2 \\ D_{GDL}, x_2 < x < x_3 \end{cases} \tag{8}$$

At the generation site, $x_2$, the flux of fluoride is considered to be balanced by the flux of fluoride away from the site by the two transport Paths (1 and 2) as shown in Eq. (9).

$$N_{F^-}\big|_{x_2} = [N_{F^-}]_{Path\,1} + [N_{F^-}]_{Path\,2} \tag{9}$$

Further, the flux of fluoride out of the GDL and into the channel is described by Eq. (10).

$$N_{F^-} = D_{GDL}\frac{dC_{F^-}}{dx} \tag{10}$$

Finally, the cumulative fluoride release into the cathode or anode channels is given by (11).

$$F_C = \int_0^t N_{F^-}\,dt \tag{11}$$

### 4.3. Ionomer thickness change

Degradation of ionomer material is considered to result only in a change in thickness, therefore the loss of a fraction of cathode

ionomer is equivalent to loosing a fraction of the cathode ionomer thickness as in Eq. (12). As the thickness changes with time, permeability can be calculated by Eq. (2).

$$\delta = \delta_{IA} + \delta^{o}_{IC} f_I \tag{12}$$

For the reinforcement layer, it is only considered a barrier to gas crossover when filled with ionomer. This model considers that radical species may reach the ionomer within half of the reinforcement layer, eventually reducing its barrier properties. This half of the reinforcement layer is included in $\delta^{o}_{IC}$.

### 4.4. Open circuit voltage

The measured voltage of an OCV durability experiment is influenced by reversible and irreversible processes [32]. Reversible processes may be affected by platinum oxidation or water content of the fuel cell while irreversible processes are affected by membrane thinning and degradation. The open circuit potential during an OCV durability test can be written as:

$$E_{OCV} = E_{Nernst} - \eta_{reversible} - \eta_{irreversible} \tag{13}$$

The irreversible loss, dominated by hydrogen crossover, can be described as:

$$\eta_{irreversible} = \eta_{Crossover} = \frac{RT}{F} \ln\left[\frac{i_{H_2}}{EAS i_o}\right] \tag{14}$$

Furthermore the total change in OCV from initial crossover and EAS conditions can be described by:

$$\Delta E_{OCV} = \frac{RT}{F} \ln\left[\frac{i^{o}_{H_2}(EAS)}{(EAS^{o}) i_{H_2}}\right] \tag{15}$$

This $\Delta E_{OCV}$ is due to irreversible losses and does not account for reversible voltage losses. Finally, the electrochemically active surface area will also decrease as the ionomer degrades as measured in a previous study [32] and seen here by the "Pt band" (in Fig. 6) causing a loss of surface platinum. A specific mechanism for this process cannot be proposed at this time. The net effect of a reduction in EAS is an increase in the crossover current on an active platinum surface area basis. As a first approximation this effect will be modeled by:

$$\Delta E_{OCV} = \frac{RT}{F} \ln\left[\frac{i^{o}_{H_2}}{i_{H_2}}\right]^{\gamma} \tag{16}$$

where $\gamma$ is a crossover current modifier which accounts for the degradation of the catalytic surface area. The above equations were solved numerically using the 'method of lines'. Initial concentrations were zero at all locations. Fluoride concentrations at the GDL/channel boundary were assumed to be zero. The initial cathode ionomer fraction, $f_I$, was unity. Parameters were determined by fitting the model to fluoride release data. Model parameters are given in Table 1. The initial hydrogen permeability, $k^{o}_{H_2}$, was measured experimentally.

## 5. Model results

The proposed degradation model was able to adequately describe the observed fluoride release trends shown in comparison to the experimental results. The model fit resulted in a fluoride ion diffusion coefficient of $7.4 \times 10^{-11}$ cm$^2$ s$^{-1}$ which shows good agreement to ion diffusion coefficients in Nafion$^{TM}$ 117 which were on the order of $2 \times 10^{-10}$ as calculated from Unnikrishnan et al. [37]. The differences in diffusion resistances in the two fluoride transport paths resulted in differences in anode and cathode fluoride release lag times as shown in Fig. 8. The slight differences

**Table 1**
Model parameters

| Variable | Value |
|---|---|
| $\Delta p$ | 364.4 mmHg |
| $\delta_{IA}$ | $7.5 \times 10^{-4}$ cm |
| $\delta^{o}_{IC}$ | $7.5 \times 10^{-4}$ cm |
| $k^{o}_{H_2}$ | $1.9 \times 10^{-8}$ A cm cm$^{-2}$ mmHg$^{-1}$ |
| $K_1$ | $1.8 \times 10^{-4}$ mol$^{-1}$ |
| $K_2$ | $4.0 \times 10^{-7}$ mol cm$^{-2}$ |
| $K_3$ | 0.7 |
| $D_{GDL}$ | $4.2 \times 10^{-9}$ cm$^2$ s$^{-1}$ |
| $D_I$ | $7.4 \times 10^{-11}$ cm$^2$ s$^{-1}$ |
| $R$ | 8.314 J mol$^{-1}$ K$^{-1}$ |
| $T$ | 363.15 K |
| $F$ | 96,485 C mol$^{-1}$ |
| $E_{Nernst} - \eta_{reversible}$ | 0.814 V |
| $\gamma$ | 2.6 |

in the experimental and modeled lag times are caused by some of the model simplifications. Degradation was considered to primarily occur at the catalyst–ionomer interface, though it may actually happen within the cathode ionomer layer. As such the resistance to ion diffusion was slightly underestimated for Path 1 in the model, resulting in a shorter lag time than experimental results. The differences in diffusion resistance also effectively captured the differences in cumulative fluoride levels after long degradation times.. Due to the increased diffusion length from the degradation location in the cathode ionomer to the anode channels, Path 2, anode cumulative release was smaller than the cathode release. Finally,

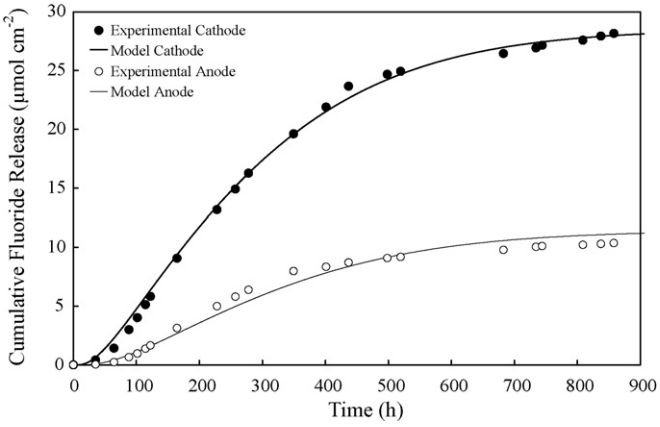


**Fig. 8.** Model and experimental fluoride release.

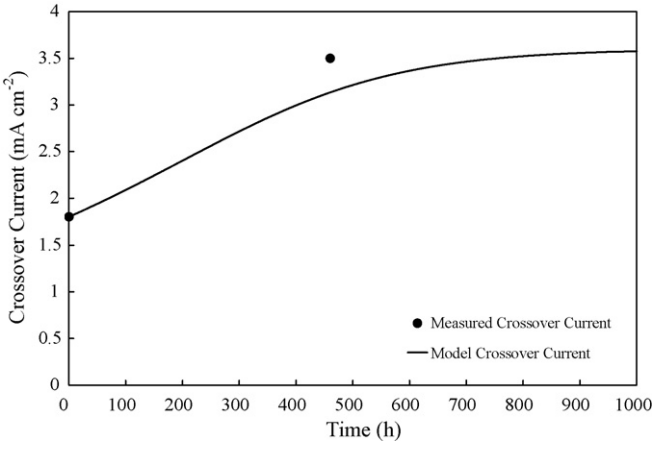


**Fig. 9.** Model and experimental hydrogen crossover results.

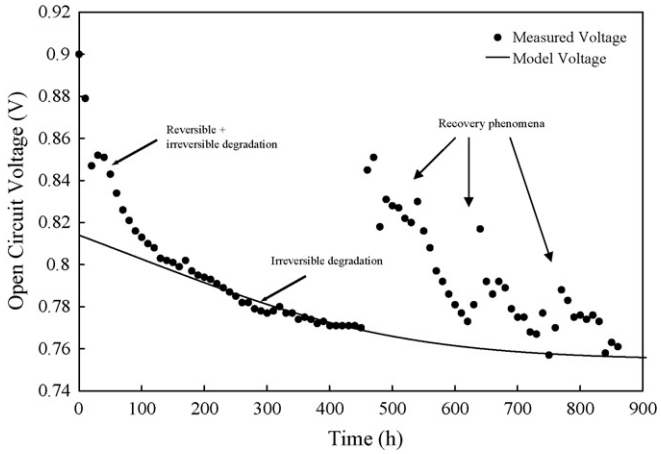


**Fig. 10.** Model and experimental OCV results.

use of the cathode ionomer fraction in the calculation for degradation and fluoride generation rate was able to model the plateau that the cumulative fluoride release curves reach.

The model also estimates hydrogen crossover. Fig. 9 is a plot of the two crossover current measurements taken during testing and the predicted crossover curves from the model. The trend cannot be confirmed due to the small number of points, however the crossover results show good agreement with the point after 460 h of operation. Note that the number of crossover current measurements was intentionally limited in order not to interfere with the OCV degradation behavior of the cell.

It has been shown in a previous publication that under open circuit conditions there are reversible voltage degradation processes which impact the open circuit voltage [32]. In the same publication voltage degradation was shown to be linked to the crossover current as well as the electrochemically active surface area. This model only considers irreversible voltage loss and attributes this loss to hydrogen crossover and loss of active surface area. Fig. 10 shows model results together with open circuit voltage data. The difference in modeled and actual voltage between 0 and 200 h is attributed to the reversible voltage loss and is on the same order of the reversible losses shown in [32]. This reversible voltage loss is not considered in the present model. After 200 h the experimental data reaches a steady degradation rate which is where the modeled voltage begins to match experimental data, except for the interruption at 460 h. After 460 h, several interruptions in testing caused voltage recovery phenomena. After each recovery incident the voltage beings to return to the steady degradation trend. Even with the added fluctuations in the voltage data the model is able to capture the overall trend.

The above results show that the proposed degradation model is able to explain the various degradation features seen in the experimental work.

## 6. Conclusions

In this study a Gore™ PRIMEA® series 5510 catalyst coated membrane was degraded using an open circuit voltage durability experiment at 90 °C, 75% anode and cathode relative humidity, and no backpressure. The forensic analysis of the membrane after 860 h of operation showed that the cathode ionomer had become severely degraded while the anode ionomer remained largely intact. A platinum band was also observed within the cathode ionomer.

Fluoride release results were also consistent with forensic results. Cathode cumulative fluoride release was much higher than anode fluoride release. With time, the anode and cathode cumulative fluoride release began to reach a plateau. The open circuit voltage data was observed to decrease with time. However, as with the cumulative fluoride release results the voltage degradation rate also slowed down.

It is proposed that all fluoride was generated through the degradation of the cathode ionomer. It is further proposed that a degradation front starts at the cathode and moves towards the ePTFE reinforcement layer. Once the cathode ionomer has been consumed the rate of fluoride generation slows as the degradation front penetrates into the inert reinforcement layer. As such cumulative fluoride release will plateau until the anode ionomer begins to degrade. Also, the rate of increase in hydrogen crossover, which is dependent on the rate of thickness reduction of the ionomer layers, will stabilize. This results in a stabilization of open circuit potential as seen experimentally for the duration of the test.

The proposed mechanism of degradation was modeled and fitted to the experimental results. The model shows that the proposed mechanism can suitably explain the observed trends. From the modeling results it is clear that the differences in anode and cathode cumulative fluoride release is due to the differences in path lengths, and consequently resistance to diffusion, that fluoride ions encounter when diffusing from the generaion point in the cathode to either the anode or cathode channels. These differences in diffusion also explain the lag times seen in the cumulative fluoride data. Further, the model is able to explain the voltage results and it shows good agreement with crossover current data.

## Acknowledgements

The authors would like to acknowledge the Natural Sciences and Engineering Research Council (NSERC) of Canada for financial support.

## References

[1] S. Kundu, M.W. Fowler, L.C. Simon, S. Grot, J. Power Sources 157 (2006) 650–656.
[2] A.B. LaConti, M. Hamdan, R.C. McDonald, in: W. Vielstich, H. Gasteiger, A. Lamm (Eds.), Handbook of Fuel Cells—Fundamentals, Technology and Applications, vol. 3, John Wiley & Sons, New York, 2003, pp. 647–663.
[3] C.H. Paik, T. Skiba, V. Mittal, S. Motupally, T.D. Jarvi, 207th Meeting of the Electrochemical Society—Meeting Abstracts, 2005, p. 771.
[4] M.F. Mathias, R. Makharia, H.A. Gasteiger, J.J. Conley, T.J. Fuller, C.J. Gittleman, S.S. Kocha, D.P. Miller, C.K. Mittelsteadt, T. Xie, S.G. Yan, P.T. Yu, Electrochem. Soc. Interface 14 (2005) 24–36.
[5] Q. Guo, Z. Qi, J. Power Sources 160 (2006) 1269–1274.
[6] E. Endoh, S. Terazono, H. Widjaja, Y. Takimoto, Electrochem. Solid-State Lett. 7 (2004) A209–A211.
[7] J. St Pierre, D.P. Wilkinson, S. Knights, M.L. Bos, J. New Mater. Electrochem. Syst. 3 (2000) 99–106.
[8] A. Collier, H. Wang, X. Zi Yuan, J. Zhang, D.P. Wilkinson, Int. J. Hydrogen Energy 31 (2006) 1838–1854.
[9] D.E. Curtin, R.D. Lousenberg, T.J. Henry, P.C. Tangeman, M.E. Tisack, J. Power Sources 131 (2004) 41–48.
[10] A. Panchenko, H. Dilger, J. Kerres, M. Hein, A. Ullrich, T. Kazc, E. Roduner, Phys. Chem. Chem. Phys. 6 (2004) 2891–2894.
[11] M. Inaba, Conference Proceedings, 14th International Conference on the Properties of Water and Steam in Kyoto, 2005, pp. 395–402.
[12] J. Healy, C. Hayden, T. Xie, K. Olson, R. Waldo, H. Gasteiger, J. Abbott, Fuel Cells 5 (2005) 302–308.
[13] M. Aoki, H. Uchida, M. Watanabe, Electrochem. Commun. 8 (2006) 1509–1513.
[14] J.J.A. Kadjo, J.P. Garnier, J.P. Maye, F. Relot, S. Martemianov, Russ. J. Electrochem. 42 (2006) 467–475.
[15] V.O. Mittal, H.R. Kunz, J.M. Fenton, J. Electrochem. Soc. 153 (2006) 1755–1759.
[16] P. Rama, R. Chen, R. Thring, Proc. Inst. Mech. Eng. Part A (J. Power Energy) 220 (2006) 535–550.
[17] M. Seddiq, H. Khaleghi, M. Mirzaei, J. Power Sources 161 (2006) 371–379.
[18] E. Arato, P. Costa, J. Power Sources 159 (2006) 861–868.
[19] K.C. Neyerlin, H.A. Gasteiger, C.K. Mittelsteadt, J. Jorne, W. Gu, J. Electrochem. Soc. 152 (2005) 1073–1080.
[20] J. Larminie, A. Dicks, Fuel Cell Systems Explained, 2nd ed., John Wiley & Sons, 2003.
[21] S. Hommura, K. Kawahara, T. Shimohira, 207th Meeting of the Electrochemical Society—Meeting Abstracts, 2005, p. 803.

[22] M. Inaba, T. Kinumoto, M. Kiriake, R. Umebayashi, A. Tasaka, Z. Ogumi, Electrochim. Acta 51 (2006) 5746–5753.
[23] V.O. Mittal, H.R. Kunz, J.M. Fenton, Electrochem. Solid-State Lett. 9 (2006) 299–302.
[24] C. Chen, T.F. Fuller, ECS Trans. 11 (2007) 1127–1137.
[25] H. Liu, J. Zhang, F.D. Coms, W. Gu, B. Litteer, H.A. Gasteiger, ECS Trans. 3 (2006) 493–505.
[26] A. Ohma, S. Suga, S. Yamamoto, K. Shinohara, ECS Trans. 3 (2006) 519–529.
[27] A. Ohma, S. Suga, S. Yamamoto, K. Shinohara, J. Electrochem. Soc. 154 (2007) 757–760.
[28] W. Bi, G.E. Gray, T.F. Fuller, Electrochem. Solid-State Lett. 10 (2007) B101–B104.
[29] E. Endoh, S. Hommura, S. Terazono, H. Widjaja, J. Anzai, ECS Trans. 1 (2008) 1083–1091.
[30] M.W. Fowler, R.F. Mann, J.C. Amphlett, B.A. Peppley, P.R. Roberge, J. Power Sources 106 (2002) 274–283.
[31] K. Teranishi, K. Kawata, S. Tsushima, S. Hirai, Electrochem. Solid-State Lett. 9 (2006) 475–477.
[32] S. Kundu, M. Fowler, L.C. Simon, R. Abouatallah, J. Power Sources 182 (2008) 254–258.
[33] S. Cleghorn, J. Kolde, W. Liu, in: W. Vielstich, H. Gasteiger, A. Lamm (Eds.), Handbook of Fuel Cells—Fundamentals, Technology and Applications, vol. 3, John Wiley & Sons, New York, 2003, pp. 566–575.
[34] S.S. Kocha, J.D. Yang, J.S. Yi, AIChE J. 52 (2006) 1916–1925.
[35] K. Broka, P. Ekdunge, J. Appl. Electrochem. 27 (1997) 117–123.
[36] W. Liu, K. Ruth, G. Rusch, J. New Mater. Electrochem. Syst. 4 (2001) 227–231.
[37] E.K. Unnikrishnan, S.D. Kumar, B. Maiti, J. Membr. Sci. 137 (1997) 133–137.